

# **Radiogenic Isotope Geology**

**ALAN P. DICKIN**

Department of Geology  
McMaster University, Hamilton, Ontario



**CAMBRIDGE**  
UNIVERSITY PRESS

PUBLISHED BY THE PRESS SYNDICATE OF THE UNIVERSITY OF CAMBRIDGE  
The Pitt Building, Trumpington Street, Cambridge, United Kingdom

CAMBRIDGE UNIVERSITY PRESS  
The Edinburgh Building, Cambridge CB2 2RU, UK  
40 West 20th Street, New York, NY 10011-4211, USA  
477 Williamstown Road, Port Melbourne, VIC 3207, Australia  
Ruiz de Alarcón 13, 28014 Madrid, Spain  
Dock House, The Waterfront, Cape Town 8001, South Africa  
<http://www.cambridge.org>

© Cambridge University Press 1995

This book is in copyright. Subject to statutory exception  
and to the provisions of relevant collective licensing agreements,  
no reproduction of any part may take place without  
the written permission of Cambridge University Press.

First published 1995  
Reprinted 1997  
First paperback edition (with corrections and additional material) 1997  
Reprinted 2000, 2002

Typeset in Monotype Times 9/11 pt

*A catalogue record for this book is available from the British Library*

*Library of Congress Cataloguing in Publication data*

Dickin, Alan P.

Radiogenic isotope geology/Alan P. Dickin.

p. cm.

Includes bibliographical references and index.

ISBN 0-521-43151-4

1. Isotope geology. 2. Radioactive dating. I. Title.

QE501.4.N9D53 1995

551.7'01-dc20 93-36765 CIP

ISBN 0 521 43151 4 hardback

ISBN 0 521 59891 5 paperback

Transferred to digital printing 2003

# CONTENTS

<i>Preface</i>	<i>xiii</i>		
<i>Acknowledgement</i>	<i>xv</i>		
<b>1 Nucleosynthesis and nuclear decay</b>	<b>1</b>		
1.1 The chart of the nuclides	1		
1.2 Nucleosynthesis	2		
1.2.1 Stellar evolution			
1.2.2 Stages in the nucleosynthesis of heavy elements			
1.3 Radioactive decay	7		
1.3.1 Isobaric decay			
1.3.2 Heavy particle decay			
1.3.3 Nuclear fission and the Oklo natural reactor			
1.4 The law of radioactive decay	11		
1.4.1 Uniformitarianism			
References	14		
<b>2 Experimental techniques</b>	<b>15</b>		
2.1 Chemical separation	15		
2.1.1 Rb–Sr			
2.1.2 Sm–Nd and Lu–Hf			
2.1.3 Lead			
2.2 Solid source mass spectrometry	19		
2.2.1 Sample loading			
2.2.2 Fractionation			
2.2.3 Ion optics			
2.2.4 Detectors			
2.2.5 Data collection			
2.2.6 Isotope dilution			
2.2.7 Double spiking			
2.3 Isochron regression line fitting	32		
2.3.1 Regression fitting with correlated errors			
2.3.2 Errorchrons			
References	36		
<b>3 The Rb–Sr method</b>	<b>39</b>		
3.1 Rb decay	39		
3.2 Dating igneous rocks	40		
3.2.1 Sr model ages			
3.2.2 The isochron diagram			
3.2.3 Erupted isochrons			
3.2.4 Meteorite chronology			
3.3 Dating metamorphic rocks	47		
3.3.1 Open mineral systems			
3.3.2 Blocking temperatures			
3.3.3 Open whole-rock systems			
3.4 Dating sedimentary rocks	53		
3.4.1 Shales			
3.4.2 Glauconite			
3.5 Seawater evolution	56		
3.5.1 Measurement of the curve			
3.5.2 Modelling of the fluxes			
References	65		
<b>4 The Sm–Nd method</b>	<b>69</b>		
4.1 Sm–Nd isochrons	69		
4.1.1 Meteorites			
4.1.2 Low-grade meta-igneous rocks			
4.1.3 High-grade metamorphic rocks			
4.1.4 High-grade metamorphic minerals			
4.2 Nd isotope evolution and model ages	78		
4.2.1 Chondritic model ages			
4.2.2 Depleted mantle model ages			
4.3 Model ages and crustal processes	85		
4.3.1 Sedimentation			
4.3.2 Metamorphism			
4.4 The crustal growth problem	90		
4.4.1 Crustal accretion ages			
4.4.2 Sediment provenance ages			
4.4.3 Archean depleted mantle			
4.5 Nd in seawater	96		
References	100		
<b>5 Lead isotopes</b>	<b>104</b>		
5.1 U–Pb isochrons	104		
5.2 U–Pb (zircon) dating	105		
5.2.1 Lead loss models			
5.2.2 Upper intersection ages			
5.2.3 Ion micro-probe analysis			
5.2.4 207/206 ages			
5.2.5 Alternative U–Pb data presentations			
5.2.6 Inherited zircon			

5.3 Common (whole-rock) Pb–Pb dating	118	7.3 Petrogenesis of continental magmas	186
5.3.1 The geochron		7.3.1 Kimberlites, carbonatites and lamproites	
5.4 Model (galena) ages	121	7.3.2 Alkali basalts	
5.4.1 The Holmes–Houtermans model		7.3.3 Flood basalts	
5.4.2 Conformable leads		7.3.4 Precambrian granitoids	
5.4.3 Open-system Pb evolution		7.3.5 Phanerozoic batholiths	
5.5 Pb–Pb dating and crustal evolution	127	References	199
References	130	8 The Re–Os system	202
6 Isotope geochemistry of oceanic volcanics	133	8.1 Analytical methods	202
6.1 Mantle heterogeneity	133	8.2 Determination of the Re decay constant	204
6.2 Isotopic tracing of mantle structure	133	8.3 Os normalisation and the Pt–Os decay scheme	207
6.2.1 Contamination and alteration		8.4 Mantle osmium	208
6.2.2 Disequilibrium melting		8.4.1 Asthenospheric evolution	
6.2.3 Mantle plumes		8.4.2 Lithospheric evolution	
6.2.4 Plum pudding mantle		8.5 Osmium as a petrogenetic tracer	216
6.2.5 Marble cake mantle		8.6 Osmium in impact sites	218
6.3 The Nd–Sr isotope diagram	141	8.7 Seawater osmium evolution	221
6.3.1 Box models for MORB sources		References	222
6.3.2 The mantle array and OIB sources		9 Specialist isotopic schemes	225
6.4 Pb isotope geochemistry	146	9.1 The Lu–Hf system	225
6.4.1 Pb–Pb isochrons and the lead paradox		9.1.1 Geochronology	
6.4.2 The terrestrial Th/U ratio		9.1.2 Mantle evolution	
6.4.3 The upper mantle $\mu$ value re-examined		9.1.3 Hf–Nd systematics of mantle depletion	
6.5 Mantle reservoirs in isotopic multispace	154	9.1.4 Hf–Nd systematics of mantle enrichment	
6.5.1 The mantle plane		9.2 The La–Ce and La–Ba systems	234
6.5.2 The mantle tetrahedron		9.2.1 La–Ba geochronology	
6.6 Identification of enriched mantle components	161	9.2.2 La–Ce geochronology	
6.6.1 HIMU		9.2.3 Ce isotope geochemistry	
6.6.2 EM II		9.3 The K–Ca system	239
6.6.3 EM I		References	243
6.6.4 Kinematic model for mantle recycling		10 K–Ar and Ar–Ar Dating	245
6.7 Island arcs and mantle evolution	164	10.1 The K–Ar dating method	245
References	169	10.1.1 Analytical techniques	
7 Isotope geochemistry of continental rocks	173	10.1.2 Inherited argon and the K–Ar isochron diagram	
7.1 Mantle xenoliths	173	10.1.3 Argon loss	
7.1.1 Mantle metasomatism		10.1.4 Calibrating the geomagnetic reversal time-scale	
7.2 Crustal contamination	178	10.2 The $^{40}\text{Ar}$ – $^{39}\text{Ar}$ dating technique	255
7.2.1 Two-component mixing models		10.2.1 Irradiation	
7.2.2 Inversion modelling of magma suites		10.2.2 Corrections	
		10.2.3 Step heating	
		10.2.4 Argon loss events	
		10.2.5 $^{39}\text{Ar}$ recoil	
		10.2.6 Dating paleomagnetism	
		10.2.7 Thermochronometry	
		10.2.8 K-feldspar thermochronometry	

10.3 Laser probe dating	270	13.6.4 $^{228}\text{Th}$	
References	274	References	358
<b>11 Rare gas geochemistry</b>	<b>277</b>	<b>14 Cosmogenic nuclides</b>	<b>360</b>
11.1 Helium	277	14.1 Carbon-14	360
11.1.1 Mass spectrometry		14.1.1 $^{14}\text{C}$ measurement by counting	
11.1.2 Helium production		14.1.2 Closed-system assumption	
11.1.3 Terrestrial primordial helium		14.1.3 Initial ratio assumption	
11.1.4 Helium and heat		14.1.4 Dendrochronology	
11.1.5 Helium and volatiles		14.1.5 Uranium series calibration	
11.1.6 Helium and non-volatiles		14.2 Accelerator mass spectrometry	369
11.2 Argon	287	14.2.1 Radiocarbon dating by AMS	
11.3 Xenon	293	14.3 Beryllium-10	372
11.4 Neon	297	14.3.1 $^{10}\text{Be}$ in the atmosphere	
References	302	14.3.2 $^{10}\text{Be}$ in soil profiles	
<b>12 U-Series dating</b>	<b>305</b>	14.3.3 $^{10}\text{Be}$ in the oceans	
12.1 Secular equilibrium and disequilibrium	305	14.3.4 $^{10}\text{Be}$ in magmatic systems	
12.2 Analytical methods	307	14.4 Chlorine-36	384
12.2.1 Alpha spectrometry		14.5 Iodine-129	386
12.2.2 Mass spectrometry		14.6 Aluminium-26	389
12.3 Daughter excess	309	14.6.1 Meteorite exposure ages	
12.3.1 $^{234}\text{U}$		14.6.2 Terrestrial exposure ages	
12.3.2 $^{230}\text{Th}$		References	393
12.3.3 $^{231}\text{Pa}$		<b>15. Extinct radionuclides</b>	<b>397</b>
12.3.4 $^{230}\text{Th}$ – $^{232}\text{Th}$		15.1 Definition	397
12.3.5 $^{231}\text{Pa}$ – $^{230}\text{Th}$		15.2 Species present in the early solar system	398
12.3.6 $^{230}\text{Th}$ sediment stratigraphy		15.2.1 Extant actinides	
12.3.7 $^{210}\text{Pb}$		15.2.2 I–Xe	
12.4 Daughter-deficiency methods	318	15.2.3 Pu–Xe	
12.4.1 $^{230}\text{Th}$ : theory		15.2.4 Al–Mg	
12.4.2 $^{230}\text{Th}$ : applications		15.2.5 Pd–Ag	
12.4.3 $^{230}\text{Th}$ : dirty calcite		15.2.6 Mn–Cr	
12.4.4 $^{231}\text{Pa}$		15.2.7 Fe–Ni	
References	327	15.3 Absent species	410
<b>13 U-Series geochemistry of igneous systems</b>	<b>330</b>	15.3.1 Cm–U	
13.1 Geochronology of volcanic rocks	330	15.3.2 Ca–K	
13.1.1 The U–Th isochron diagram		References	411
13.2 Magma chamber evolution	332	<b>16 Fission track dating</b>	<b>413</b>
13.2.1 The Th isotope evolution diagram		16.1 Track formation	413
13.3 Melting models	335	16.2 Track etching	415
13.3.1 Ocean island volcanics		16.3 Counting techniques	416
13.3.2 Ocean ridge processes		16.3.1 Population method	
13.3.3 The Th–U isochron diagram		16.3.2 External detector method	
13.3.4 U–Th model age dating		16.3.3 Re-etching method	
13.3.5 Genesis of oceanic granites		16.3.4 Re-polishing method	
13.4 Mantle evolution	344	16.4 Detrital populations	419
13.5 Subduction zone processes	347	16.5 Track annealing	420
13.6 Short-lived U-series isotopes	351	16.6 Uplift and subsidence rates	422
13.6.1 $^{226}\text{Ra}$		16.7 Track length measurements	425
13.6.2 $^{231}\text{Pa}$		References	434
13.6.3 $^{228}\text{Ra}$		<b>Appendix A: Chart of the nuclides</b>	<b>437</b>
		<b>Appendix B: Updated material for the 1997 paperback edition</b>	<b>441</b>
		<i>Index</i>	479

# 1 Nucleosynthesis and nuclear decay

## 1.1 The chart of the nuclides

In the field of isotope geology, neutrons, protons and electrons can be regarded as the fundamental building blocks of the atom. The composition of a given type of atom, called a nuclide, is described by specifying the number of protons (atomic number,  $Z$ ) and the number of neutrons ( $N$ ) in the nucleus. The sum of these is the mass number ( $A$ ). By plotting  $Z$  against  $N$  for all of the nuclides that have been known to exist (at least momentarily), the chart of the nuclides is

obtained (Fig. 1.1). In this chart, horizontal rows of nuclides represent the same element (constant  $Z$ ) with a variable number of neutrons ( $N$ ). These are isotopes.

Presently 264 stable nuclides are known, which have not been observed to decay (with available detection equipment). These define a central 'path of stability', coloured black in Fig. 1.1. On either side of this path, the zig-zag outline defines the limits of experimentally known unstable nuclides (Hansen, 1987). These tend to undergo increasingly rapid

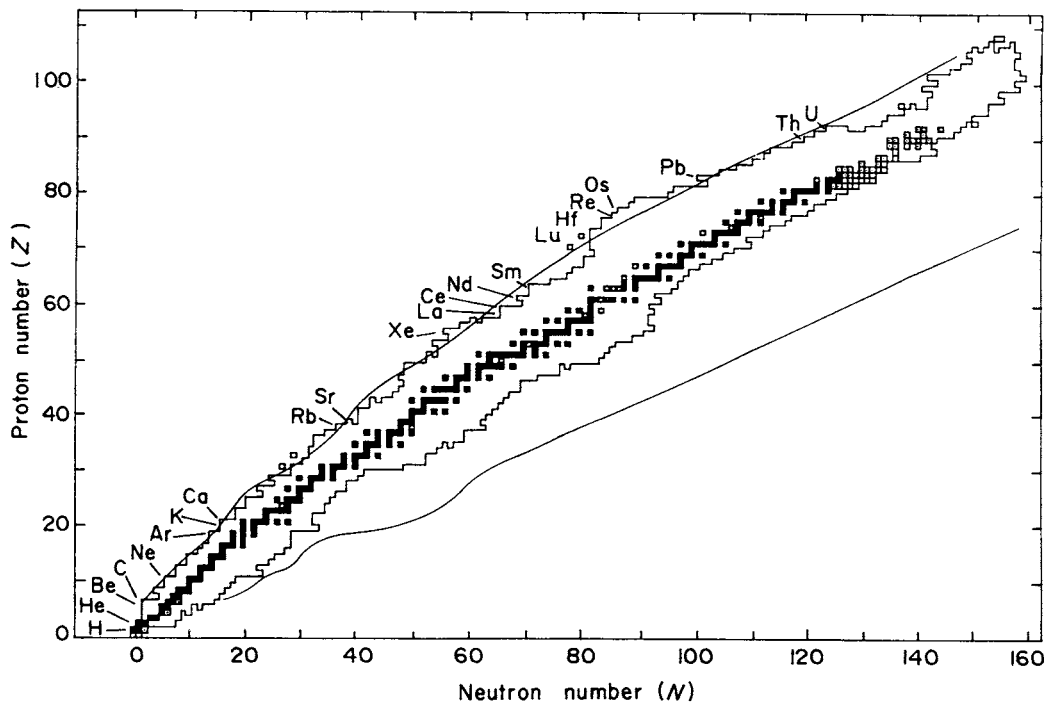


Fig. 1.1. Chart of the nuclides in coordinates of proton number,  $Z$ , against neutron number,  $N$ . (■) = stable nuclides; (□) = unstable nuclides; (◻) = naturally occurring long-lived unstable nuclides; (◻) = naturally occurring short-lived unstable nuclides. Some geologically useful radionuclides are marked. Smooth envelope = theoretical nuclide stability limits. For a more detailed nuclide chart, see the appendix A.

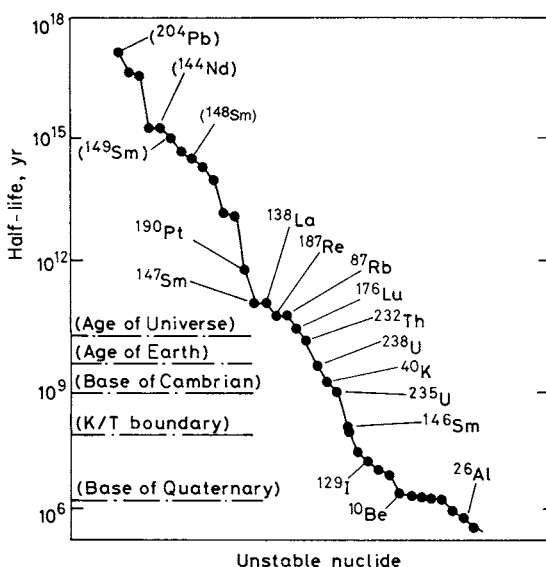


Fig. 1.2. Unstable nuclides with half-lives ( $t_{1/2}$ ) over 0.5 Myr, in order of decreasing stability. Geologically useful parent nuclides are marked. Some very long-lived radionuclides with no geological application are also marked, in brackets.

decay as one moves out on either side of the path of stability. The smooth outer envelopes are the theoretical limits of nuclide stability, beyond which 'prompt' decay occurs. In that case the synthesis and decay of an unstable nuclide occurs in a single particle interaction, giving it a zero effective lifetime. As work progresses, the domain of experimentally known nuclides should approach the theoretical envelope, as has already occurred for nuclides with  $Z < 22$  (Hansen, 1987).

A small number of unstable nuclides have sufficiently long half-lives that they have not entirely decayed to extinction since the formation of the solar system. A few other short-lived nuclides are either continuously generated in the decay series of uranium and thorium, or produced by cosmic ray bombardment of stable nuclides. These nuclides, and one or two extinct short-lived isotopes, plus their daughter products, are the realm of radiogenic isotope geology. Those with half-lives over 0.5 Myr are marked in Fig. 1.2. Nuclides with half-lives over  $10^{12}$  yr decay too slowly to be geologically useful. Observation shows that all of the other long-lived isotopes either have been or are being applied in geology.

## 1.2 Nucleosynthesis

A realistic model for the nucleosynthesis of the elements must be based on empirical data for their 'cosmic abundance'. True cosmic abundances can be derived from stellar spectroscopy or by chemical analysis of galactic cosmic rays. However, such data are difficult to measure at high precision, so cosmic abundances are normally approximated by solar-system abundances. These can be determined by solar spectroscopy or by direct analysis of the most 'primitive' meteorites, carbonaceous chondrites. A comparison of the latter two sources of data (Ross and Aller, 1976) demonstrates good agreement for most elements (Fig. 1.3). Exceptions are the volatile elements, which have been lost from meteorites, and the Li-Be-B group, which are unstable in stars.

It is widely believed (e.g. Weinberg, 1977) that about 30 minutes after the 'hot big bang', the matter of the universe (in the form of protons and neutrons) consisted mostly of  $^1\text{H}$  and 22–28% by mass of  $^4\text{He}$ , along with traces of  $^2\text{H}$  (deuterium) and  $^3\text{He}$ . Hydrogen is still by far the most abundant element in the universe (88.6% of all nuclei) and with helium, makes up 99% of its mass, but naturally occurring heavy nuclides now exist up to atomic weight 254 or beyond (Fig. 1.1). These heavier nuclei must have been produced by nucleosynthetic processes in stars, and not in the big bang, because stars of different ages have different compositions which can be detected spectroscopically. Furthermore, stars at particular evolutionary stages may have compositional abnormalities, such as the presence of  $^{254}\text{Cf}$  in supernovae. If nucleosynthesis of the heavy elements had occurred in the big bang then their distribution would be uniform about the universe.

### 1.2.1 Stellar evolution

Present-day models of stellar nucleosynthesis are based heavily on a classic review paper by Burbidge *et al.* (1957), in which eight element-building processes were identified (hydrogen burning, helium burning,  $\alpha$ , e, s, r, x and p). Different processes were invoked to explain the abundance patterns of different groups of elements. These processes are, in turn, linked to different stages of stellar evolution. It is therefore appropriate at this point to summarise the life-history of some typical stars (e.g. Iben, 1967). The length of this life-history depends directly on the stellar mass, and can be traced on a plot of absolute magnitude (brightness) against spectral class (colour), referred to as the Hertzsprung-Russell or H-R diagram (Fig. 1.4).

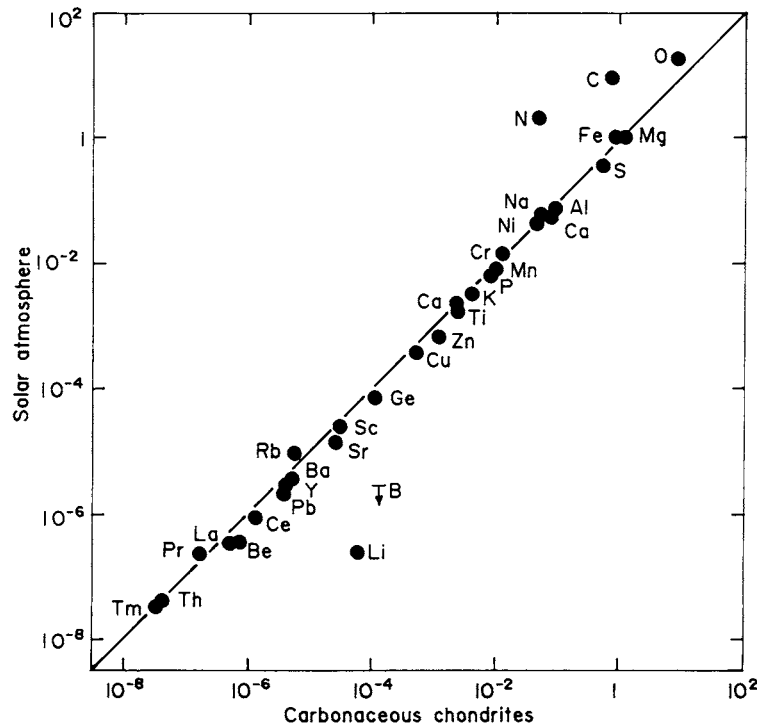


Fig. 1.3. Comparison of solar-system abundances (relative to silicon) determined by solar spectroscopy and by analysis of carbonaceous chondrites. After Ringwood (1979).

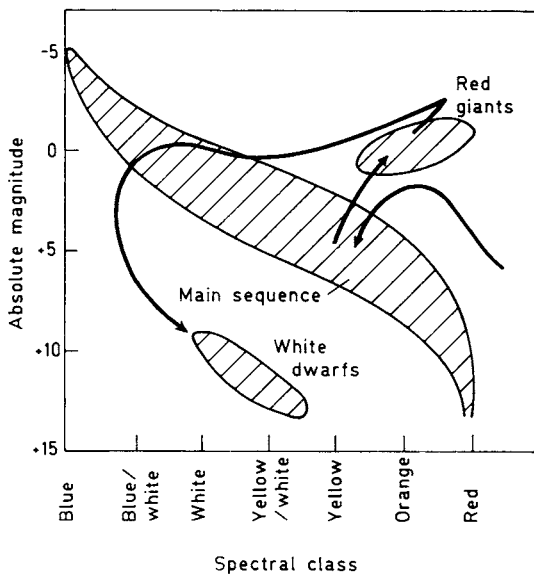


Fig. 1.4. Plot of absolute magnitude against spectral class of stars. Hatched areas show distributions of the three main star groups. The postulated evolutionary path of a star of solar mass is shown.

Gravitational accretion of a star of solar mass from cold primordial hydrogen and helium would probably take about  $10^6$  yr to raise the core temperature to ca.  $10^7$  K, when nuclear fusion of hydrogen to helium can begin (Atkinson and Houtermans, 1929). This process is also called 'hydrogen burning'. The star spends most of its life at this stage, as a 'Main Sequence' star, where equilibrium is set up between energy supply by fusion and energy loss in the form of radiation. For the Sun, this stage will probably last ca.  $10^{10}$  yr, but a very large star with 15 times the Sun's mass may remain in the Main Sequence for only  $10^7$  yr.

When the bulk of hydrogen in a small star has been converted into  $^4\text{He}$ , inward density-driven forces exceed outward radiation pressure, causing gravitational contraction. However, the resulting rise in core temperature causes expansion of the outer hydrogen-rich layer of the star. This forms a huge low-density envelope whose surface temperature may fall to ca. 4000 K, observed as a 'Red Giant'. This stage lasts only one-tenth as long as the Main Sequence stage. When core temperatures reach  $1.5 \times 10^7$  K, a more efficient hydrogen-burning reaction becomes possible if the star contains traces of carbon, nitrogen and



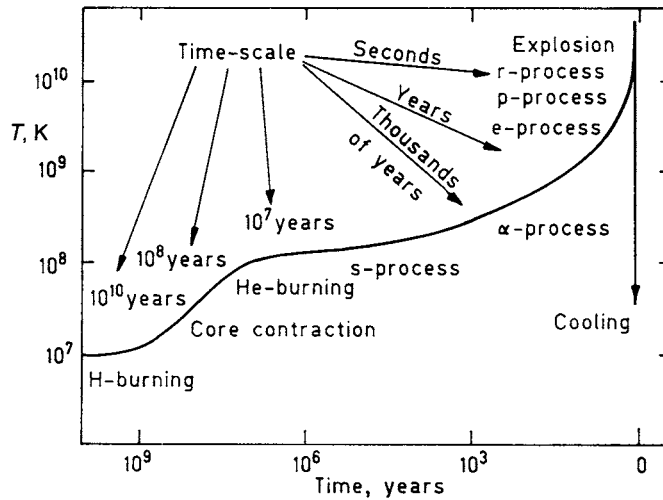


Fig. 1.5. Schematic diagram of the evolution of a large star showing the nucleosynthetic processes that occur along its accelerating life-history in response to increasing temperature ( $T$ ). Note that time is measured backwards from the end of the star's life on the right. After Burbidge *et al.* (1957).

oxygen inherited from older generations of stars. This form of hydrogen burning is called the CNO cycle (Bethe, 1939).

At some point during the Red Giant stage, core temperatures may reach  $10^8$  K, when He fusion to carbon is ignited (the 'helium flash'). Further core contraction, yielding a temperature of ca.  $10^9$  K, follows as helium becomes exhausted. At these temperatures an endothermic process of  $\alpha$ -particle emission can occur, allowing the building of heavier nuclides up to mass 40. However, this quickly expends the remaining burnable fuel of the star, which then cools to a White Dwarf.

More massive stars (of several solar masses) have a different life-history. In these stars, the greater gravitationally induced pressure-temperature conditions allow the fusion of helium to begin early in the Red Giant stage. This is followed by further contraction and heating, allowing the fusion of carbon and successively heavier elements. However, as lighter elements become exhausted, gravitationally induced contraction and heating occur at an ever increasing pace (Fig. 1.5), until the implosion is stopped by the attainment of neutron-star density. The resulting shock wave causes a supernova explosion which ends the star's life.

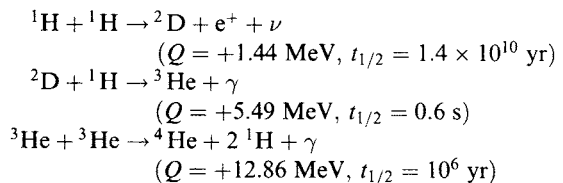
In the minutes before explosion, when temperatures exceed  $3 \times 10^9$  K, very rapid nuclear interactions occur. Energetic equilibrium is established between nuclei and free protons and neutrons, synthesising elements like Fe by the so-called e-process. The

supernova explosion itself lasts only a few seconds, but is characterised by colossal neutron fluxes. These very rapidly synthesise heavier elements, terminating at  $^{254}\text{Cf}$ , which undergoes spontaneous fission. Products of the supernova explosion are distributed through space and later incorporated in a new generation of stars.

### 1.2.2 Stages in the nucleosynthesis of heavy elements

A schematic diagram of the cosmic abundance chart is given in Fig. 1.6. We will now see how different nucleosynthetic processes are invoked to account for its form.

The element-building process begins with the fusion of four protons to one  $^4\text{He}$  nucleus, which occurs in three stages:



where  $Q$  is the energy output and  $t_{1/2}$  is the reaction time of each stage (the time necessary to consume one-half of the reactants) for the centre of the Sun. The long reaction time for the first step explains the long duration of the hydrogen-burning (Main Sequence) stage for small stars like the Sun. The

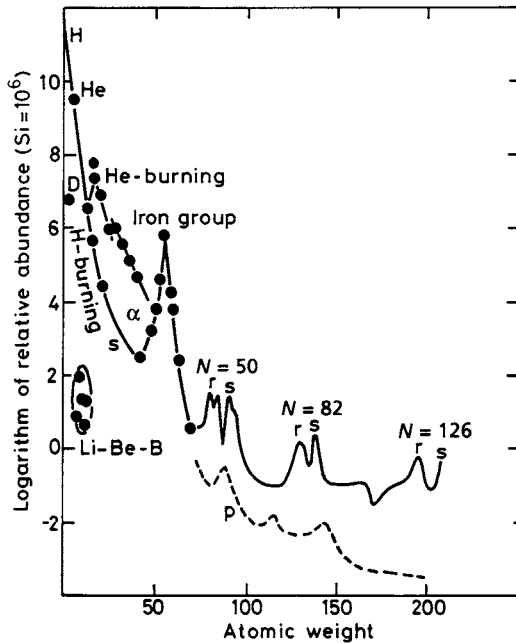
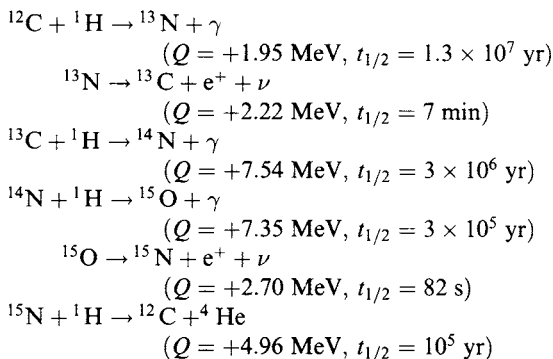


Fig. 1.6. Schematic diagram of the cosmic abundances of the elements, highlighting the nucleosynthetic processes responsible for forming different groups of nuclides. After Burbidge *et al.* (1957).

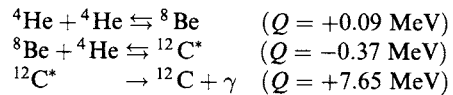
overall reaction converts four protons into one helium nucleus, two positrons and two neutrinos, plus a large output of energy in the form of high frequency photons. Hence the reaction is very strongly exothermic. Although deuterium and  $^3\text{He}$  are generated in the first two reactions above, their consumption in the third accounts for their much lower cosmic abundance than  $^4\text{He}$ .

If heavier elements are present in a star (e.g. carbon and nitrogen) then the catalytic C–N–O sequence of reactions can occur, which also combines four protons to make one helium nucleus:



The C–N–O elements have greater potential energy barriers to fusion than hydrogen, so these reactions require higher temperatures to operate than the simple proton–proton (p–p) reaction. However, the reaction times are much shorter than for the p–p reaction. Therefore the C–N–O reaction contributes less than 10% of hydrogen-burning reactions in a small star like the Sun, but is overwhelmingly dominant in large stars. This explains their much shorter lifespan in the Main Sequence.

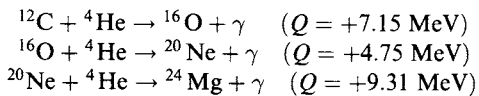
Helium burning also occurs in stages:



The  $^8\text{Be}$  nucleus is very unstable ( $t_{1/2} < 10^{-15} \text{ s}$ ) and in the core of a Red Giant the Be/He equilibrium ratio is estimated at  $10^{-9}$ . However its life is just long enough to allow the possibility of collision with another helium nucleus. (Instantaneous 3-particle collisions are very rare). The energy yield of the first stage is small, and the second is actually endothermic, but the decay of excited  $^{12}\text{C}^*$  to the ground state is strongly exothermic, driving the equilibria to the right.

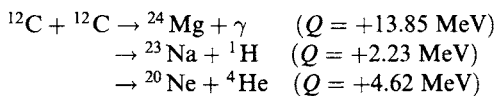
The elements Li, Be and B have low nuclear binding energies, so that they are unstable at the temperatures of  $10^7 \text{ K}$  and above found at the centres of stars. They are therefore bypassed by stellar nucleosynthetic reactions, leading to low cosmic abundances (Fig. 1.6). The fact that the five stable isotopes  $^6\text{Li}$ ,  $^7\text{Li}$ ,  $^9\text{Be}$ ,  $^{10}\text{B}$  and  $^{11}\text{B}$  exist at all has been attributed to fragmentation effects (spallation) of heavy cosmic rays (atomic nuclei travelling through the galaxy at relativistic speeds) as they hit interstellar gas atoms (Reeves, 1974). This is termed the x-process.

Following the synthesis of carbon, further helium-burning reactions are possible, to produce heavier nuclei:



Intervening nuclei such as  $^{13}\text{N}$  can be produced by adding protons to these species, but are themselves consumed in the process of catalytic hydrogen burning mentioned above.

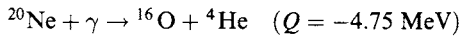
In old Red Giant stars, carbon-burning reactions can occur:



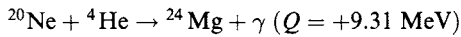
## 6 1 Nucleosynthesis and nuclear decay

The hydrogen and helium nuclei regenerated in these processes allow further reactions which help to fill in gaps between masses 12 and 24.

When a small star reaches its maximum core temperature of  $10^9$  K the endothermic  $\alpha$ -process can occur:



The energy consumption of this process is compensated by strongly exothermic reactions such as:

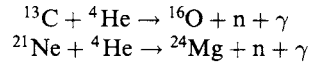


so that the overall reaction generates a positive energy budget. The process resembles helium burning, but is distinguished by the different source of  $^4\text{He}$ . The  $\alpha$ -process can build up from  $^{24}\text{Mg}$  through the sequence  $^{28}\text{Si}$ ,  $^{32}\text{S}$ ,  $^{36}\text{Ar}$  and  $^{40}\text{Ca}$ , where it terminates, owing to the instability of  $^{44}\text{Ti}$ .

The maximum temperatures reached in the core of a small star do not allow substantial heavy-element production. However, in the final stages of the evolution of larger stars, before a supernova explosion, the core temperature exceeds  $3 \times 10^9$  K. This allows energetic equilibrium to be established by very rapid nuclear reactions between the various nuclei and free protons and neutrons (the e-process). Because  $^{56}\text{Fe}$  is at the peak of the nuclear binding-energy curve, this element is most favoured by the e-process (Fig. 1.6). However, the other first-series

transition elements V, Cr, Mn, Co and Ni in the mass range 50 to 62 are also attributed to this process.

During the last few million years of a Red Giant's life, a slow process of neutron addition with emission of  $\gamma$  rays (the s-process) can synthesise many additional nuclides up to mass 209 (see Fig. 1.7). Two possible neutron sources are:



The  $^{13}\text{C}$  and  $^{21}\text{Ne}$  parents can be produced by proton bombardment of the common  $^{12}\text{C}$  and  $^{20}\text{Ne}$  nuclides.

Because neutron capture in the s-process is relatively slow, unstable neutron-rich nuclides generated in this process have time to decay by  $\beta$  emission before further neutron addition. Hence the nucleosynthetic path of the s-process climbs in many small steps up the path of greatest stability of proton/neutron ratio (Fig. 1.7) and is finally terminated by the  $\alpha$  decay of  $^{210}\text{Po}$  back to  $^{206}\text{Pb}$  and  $^{209}\text{Bi}$  back to  $^{205}\text{Tl}$ .

The 'neutron capture cross-section' of a nuclide expresses how readily it can absorb incoming thermal neutrons, and therefore determines how likely it is to be converted to a higher atomic mass species by neutron bombardment. Nuclides with certain neutron numbers (e.g. 50, 82 and 126) have unusually small neutron capture cross-sections, making them particularly resistant to further reaction and giving rise to local peaks in abundance at masses 90, 138 and 208.

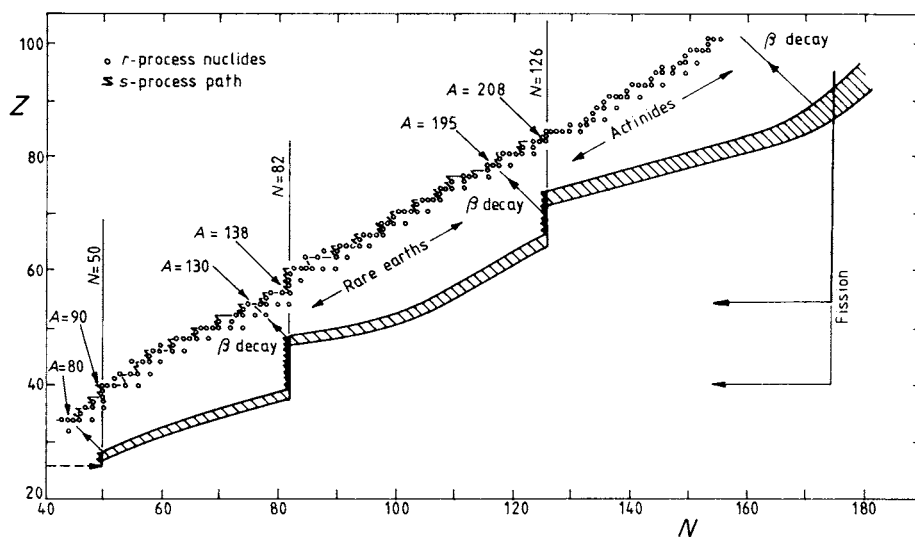


Fig. 1.7. Neutron capture paths of the s-process and r-process shown on the chart of the nuclides. Hatched zone indicates the r-process nucleosynthetic pathway for a plausible neutron flux. Neutron 'magic numbers' are indicated by vertical lines, and mass numbers of nuclide abundance peaks are marked. After Seeger *et al.* (1965).

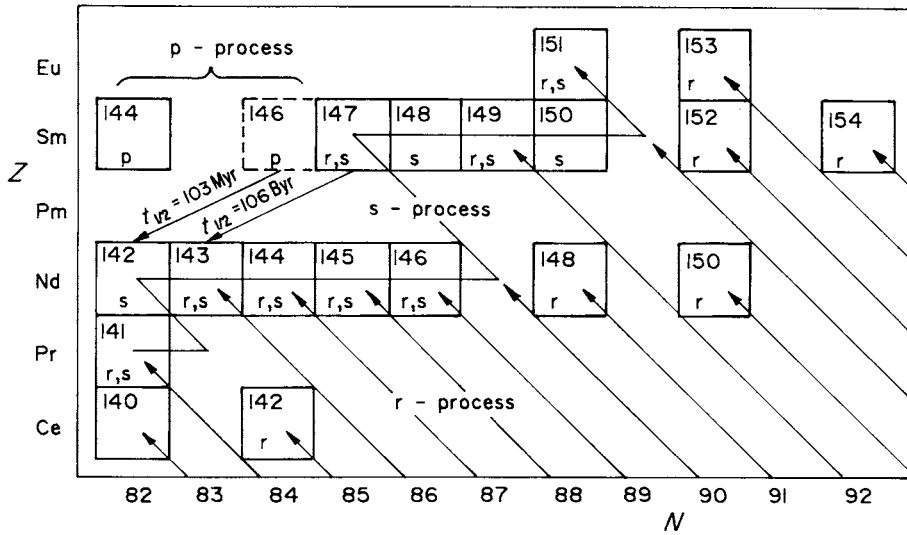


Fig. 1.8. Part of the chart of the nuclides in the area of the light rare earths to show p-, r- and s-process product nuclides. After O’Nions *et al.* (1979).

$N = 50, 82$  and  $126$  are empirically referred to as neutron ‘magic numbers’.

In contrast to the s-process, which may occur over periods of millions of years in Red Giants, r-process neutrons are added in very rapid succession to a nucleus before  $\beta$  decay is possible. The nuclei are therefore rapidly driven to the neutron-rich side of the stability line, until they reach a new equilibrium between neutron addition and  $\beta$  decay, represented by the hatched zone in Fig. 1.7. Nuclides move along this r-process pathway until they reach a configuration with low neutron capture cross-section (a neutron magic number). At these points a ‘cascade’ of alternating  $\beta$  decays and single neutron additions occurs, indicated by the notched ladders in Fig. 1.7. Nuclides climb these ladders until they reach the next segment of the r-process pathway.

Nuclides with neutron magic numbers build to excess abundances, as with the s-process, but they occur at proton-deficient compositions relative to the s-process stability path. Therefore, when the neutron flux falls off and nuclides on the ladders undergo  $\beta$  decay back to the stability line, the r-process local abundance peaks are displaced about 6–12 mass units below the s-process peaks (Fig. 1.6).

The r-process is terminated by neutron-induced fission at mass 254, and nuclear matter is fed back into the element-building processes at masses of ca. 108 and 146. Thus, cycling of nuclear reactions occurs above mass 108. Because of the extreme neutron flux

postulated for the r-process, its occurrence is probably limited to supernovae.

The effects of r- and s-process synthesis of typical heavy elements may be demonstrated by an examination of the chart of the nuclides in the region of the light rare earths (Fig. 1.8). The step by step building of the s-process contrasts with the ‘rain of nuclides’ produced by  $\beta$  decay of r-process products. Some nuclides, such as  $^{143}\text{Nd}$  to  $^{146}\text{Nd}$  are produced by both r- and s-processes. Some, such as  $^{142}\text{Nd}$  are s-only nuclides ‘shielded’ from the decay products of the r-process by intervening nuclides. Others, such as  $^{148}\text{Nd}$  and  $^{150}\text{Nd}$  are r-only nuclides which lie off the s-process production pathway.

Several heavy nuclides from  $^{74}\text{Se}$  to  $^{196}\text{Hg}$  lie isolated on the proton-rich side of the s-process growth path (e.g.  $^{144}\text{Sm}$  in Fig. 1.8), and are also shielded from r-process production. In order to explain the existence of these nuclides it is necessary to postulate a p-process by which normal r- and s-process nuclei are bombarded by protons at very high temperature ( $> 2 \times 10^9\text{K}$ ), probably in the outer envelope of a supernova.

### 1.3 Radioactive decay

Nuclear stability and decay is best understood in the context of the chart of nuclides. It has already been noted that naturally occurring nuclides define a path in the chart of the nuclides, corresponding to the

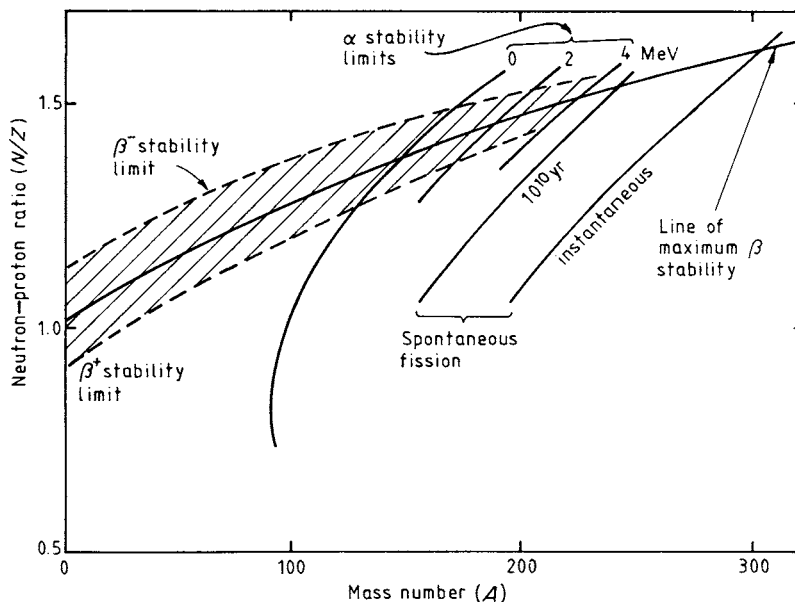


Fig. 1.9. Theoretical stability limits of nuclides illustrated on a plot of  $N/Z$  against mass number ( $A$ ). Lower limits for  $\alpha$  emission are shown for  $\alpha$  energies of 0, 2 and 4 MeV. Stability limits against spontaneous fission are shown for half-lives of  $10^{10}$  yr and zero (instantaneous fission). After Hanna (1959).

greatest stability of proton/neutron ratio. For nuclides of low atomic mass, the greatest stability is achieved when the number of neutrons and protons are approximately equal ( $N = Z$ ) but as atomic mass increases, the stable neutron/proton ratio increases until  $N/Z = 1.5$ . Theoretical stability limits are illustrated on a plot of  $N/Z$  against mass number ( $A$ ) in Fig. 1.9 (Hanna, 1959).

The path of stability is in fact an energy 'valley' into which the surrounding unstable nuclides tend to fall, emitting particles and energy. This constitutes the process of radioactive decay. The nature of particles emitted depends on the location of the unstable nuclide relative to the energy valley. Unstable nuclides on either side of the valley usually decay by 'isobaric' processes. That is, a nuclear proton is converted to a neutron, or vice-versa, but the mass of the nuclide does not change significantly (except for the 'mass defect' consumed as nuclear binding energy). In contrast, unstable nuclides at the high end of the energy valley often decay by emission of a heavy particle (e.g.  $\alpha$  particle), thus reducing the overall mass of the nuclide.

### 1.3.1 Isobaric decay

Different decay processes indicated on Fig. 1.9 can best be understood by looking at example sections of

the chart of nuclides. Figure 1.10 shows a part of the chart around the element potassium. The diagonal lines indicate isobars (nuclides of equal mass) which are displayed on energy sections in Fig. 1.11 and Fig. 1.12.

Nuclides deficient in protons decay by transformation of a neutron into a proton and an electron. The latter is then expelled from the nucleus as a negative ' $\beta$ ' particle ( $\beta^-$ ), along with an anti-neutrino ( $\bar{\nu}$ ). The energy released by the transformation is divided between the  $\beta$  particle and the anti-neutrino as kinetic energy (Fermi, 1934). The observed consequence is that the  $\beta$  particles emitted have a continuous energy distribution from nearly zero to the maximum decay energy. Low-energy  $\beta$  particles are very difficult to separate from background noise in a detector, making the  $\beta$  decay constant of nuclides such as  $^{87}\text{Rb}$  very difficult to determine accurately by direct counting (section 3.1).

In many cases the nuclide produced by  $\beta$  decay is left in an excited state which subsequently decays to the ground state nuclide by a release of energy. This may either be lost as a  $\gamma$  ray of discrete energy, or may be transferred from the nucleus to an orbital electron, which is then expelled from the atom. In the latter case, nuclear energy emission in excess of the binding energy of the electron is transferred to the electron as kinetic energy, which is superimposed as a line

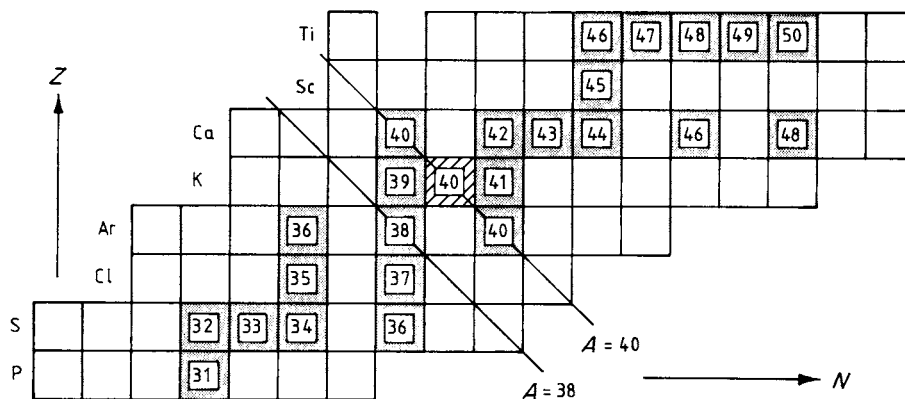


Fig. 1.10. Part of the chart of the nuclides, in coordinates of atomic number ( $Z$ ) against neutron number ( $N$ ) in the region of potassium. Stable nuclides are shaded; the long-lived unstable nuclide  $^{40}\text{K}$  is hatched. Diagonal lines are isobars (lines of constant mass number,  $A$ ).

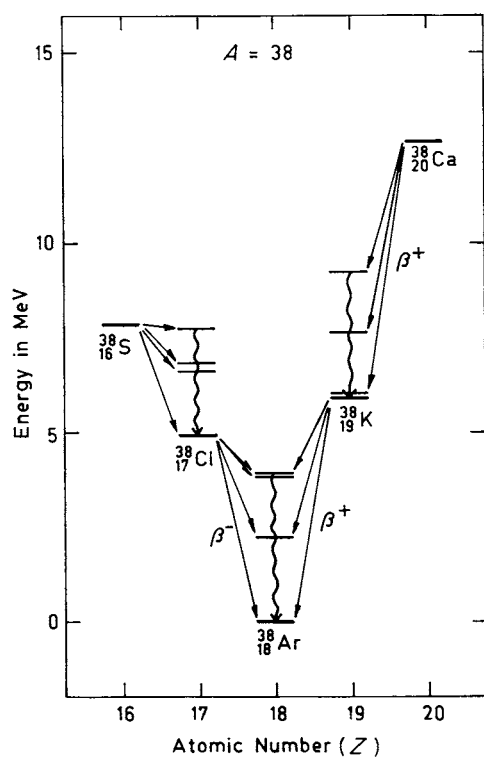


Fig. 1.11. A simple energy section through the chart of nuclides along the isobar  $A = 38$  showing nuclides and isomers. Data from Lederer and Shirley (1978).

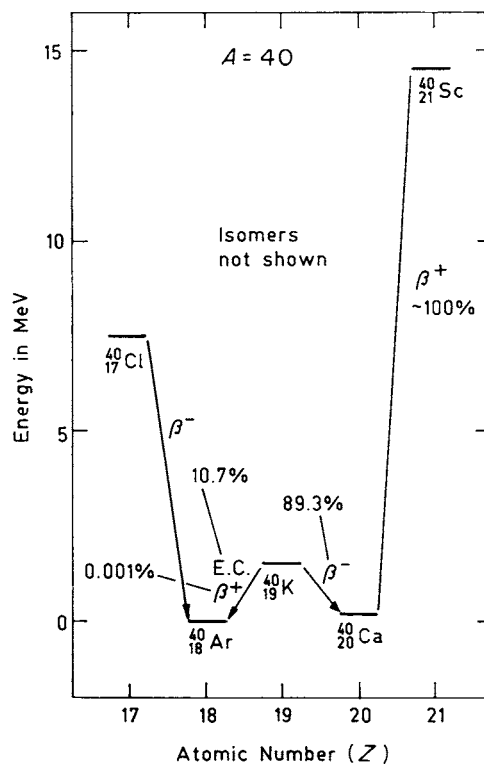


Fig. 1.12. Energy section through the chart of nuclides along isobar  $A = 40$ . Isomers are omitted for simplicity. For nuclides with more than one decay mechanism the percentage of transitions by different decay routes is indicated. Data from Lederer and Shirley (1978).

spectrum on the continuous spectrum of the  $\beta$  particles. The meta-stable states, or 'isomers' of the product nuclide are denoted by the superfix 'm', and have half-lives from less than a picosecond up to 241 years (in the case of  $^{192\text{m}}\text{Ir}$ ). Many  $\beta$  emitters have complex energy spectra involving a ground state product and more than one short-lived isomer, as shown in Fig. 1.11. The decay of  $^{40}\text{Cl}$  can yield 35 different isomers of  $^{40}\text{Ar}$  (Lederer and Shirley, 1978), but these are omitted from Fig. 1.12 for the sake of clarity.

Nuclides deficient in neutrons, e.g.  $^{38}\text{K}$  (Fig. 1.11), may decay by two different processes: positron emission and electron capture. Both processes yield a product nuclide which is an isobar of the parent, by transformation of a proton to a neutron. In positron emission a positively charged electron ( $\beta^+$ ) is emitted from the nucleus along with a neutrino. As with  $\beta^-$  emission, the decay energy is shared between the kinetic energy of the two particles. After having been slowed down by collision with atoms, the positron interacts with an orbital electron, whereby both are annihilated, yielding two 0.511 MeV  $\gamma$  rays. (This forms part of the decay energy of the nuclear transformation.)

In electron capture decay (E.C.) a nuclear proton is transformed into a neutron by capture of an orbital electron, usually from one of the inner shells, but possibly from an outer shell. A neutrino is emitted from the nucleus, and an outer orbital electron falls into the vacancy produced by electron capture, emitting a characteristic x-ray. The product nucleus may be left in an excited state, in which case it decays to the ground state by  $\gamma$  emission.

When the transition energy of a decay route is less than the energy equivalent of the positron mass ( $2m_e c^2 = 1.022$  MeV), decay is entirely by electron capture. Thereafter, the ratio  $\beta^+/\text{E.C.}$  increases rapidly with increasing transition energy (Fig. 1.12), but a small amount of electron capture always accompanies positron emission even at high transition energies.

It is empirically observed (Mattauch, 1934) that adjacent isobars cannot be stable. Since  $^{40}\text{Ar}$  and  $^{40}\text{Ca}$  are both stable species (Fig. 1.10),  $^{40}\text{K}$  must be unstable, and exhibits a branched decay to the isobars on either side (Fig. 1.12).

### 1.3.2 Heavy particle decay

Heavy atoms above bismuth in the chart of nuclides often decay by emission of an  $\alpha$  particle, consisting of two protons and two neutrons ( $\text{He}^{++}$ ). The daughter

product is not an isobar of the parent, and has an atomic mass reduced by four. The product nuclide may be in the ground state, or remain in an excited state and subsequently decay by  $\gamma$  emission. The decay energy is shared between kinetic energy of the  $\alpha$  particle and recoil energy of the product nuclide.

The U and Th decay series are shown in Fig. 12.1. Because the energy valley of stable proton/neutron ratios in this part of the chart of the nuclides has a slope of less than unity,  $\alpha$  decays tend to drive the products off to the neutron-rich side of the energy valley, where they undergo  $\beta$  decay. In fact  $\beta$  decay may occur before the corresponding  $\alpha$  decay.

At intermediate masses in the chart of the nuclides,  $\alpha$  decay may occasionally be an alternative to positron or electron capture decay for proton-rich species such as  $^{147}\text{Sm}$ . However,  $\alpha$  decays do not occur at low atomic numbers because the path of nuclear stability has a  $Z/N$  slope close to unity in this region (Fig. 1.1). Any such decays would simply drive unstable species along (parallel to) the energy valley.

A new kind of radioactive decay has recently been discovered in the  $^{235}\text{U}$  to  $^{207}\text{Pb}$  decay series (Rose and Jones, 1984), whereby  $^{223}\text{Ra}$  decays by emission of  $^{14}\text{C}$  directly to  $^{209}\text{Pb}$  with a decay energy of 13.8 MeV. However this mode of decay occurs with a frequency of less than  $10^{-9}$  of the  $\alpha$  decay of  $^{223}\text{Ra}$ .

### 1.3.3. Nuclear fission and the Oklo natural reactor

The nuclide  $^{238}\text{U}$  (atomic no. 92) undergoes spontaneous fission into two product nuclei of different atomic number, typically ca. 40 and 55 (Zr and Cs), along with various other particles and a large amount of energy. Because the heavy parent nuclide has a high neutron/proton ratio, the daughter products have an excess of neutrons and undergo isobaric decay by  $\beta$  emission. Although the frequency of spontaneous fission of  $^{238}\text{U}$  is less than  $2 \times 10^{-6}$  that of  $\alpha$  decay, in heavier transuranium elements spontaneous fission is the principal mode of decay. Other nuclides, such as  $^{235}\text{U}$ , may undergo fission if they are struck by a neutron. Furthermore, since fission releases neutrons which promote further fission reactions, a chain reaction may be established. If the concentration of fissile nuclides is high enough, this leads to a thermonuclear explosion, as in a supernova or atomic bomb.

In special cases where an intermediate heavy-element concentration is maintained, a self-sustaining but non-explosive chain reaction may be possible. This depends largely on the presence of a 'moderator'.